VIP *Very Important Paper*

Special Collection

The Modified Liquid-Liquid Interface: The Effect of an Interfacial Layer of MoS_2 on Ion Transfer

Hussain A. Al Nasser,[a] Mark A. Bissett,[b, c] and Robert A. W. Dryfe*[a, c]

MoS_2 nanosheets have been assembled at the water | 1,2-dichlorobenzene (DCB) interface into uniform films, and the ion-transfer properties investigated by voltammetry at the interface between immiscible electrolyte solutions. Remarkably, interfacial MoS_2 films were found to enhance the simple and facilitated transfer of cationic species while restricting the transport of anionic species. The enhancement is attributed to a localised increase in the cationic concentration at the interface due to the adsorption onto the negatively charged surface of the exfoliated MoS_2 nanosheets. Size-selectivity for the cationic species was also recognized as a feature of such films. Characterisation of the interfacial film's structure revealed the inclusion of multiple emulsified droplets stabilised by MoS_2, where the droplet number and size depend on the concentration of the MoS_2 dispersion. Besides increasing the interfacial corrugation and area, the emulsified droplets are believed to influence the mass transport mechanism across the interface. Cyclic voltammetric measurements of saturated films suggested a capillary-like structure of these films. While the capillaries/nanochannels allow them to have a degree of size-selectivity that depends on the thickness/density of the film, they also affect the diffusion zones towards and away from the interface. Consequently, steady-state conditions of mass transport similar to those found in solid-state supported micro-ITIES are observed in these nanofilms.

1. Introduction

In the last few decades, considerable effort has been directed towards the study of the interface between two immiscible electrolyte solutions (ITIES) owing to the intrinsic interest in charge transfer at this class of interface, and to mooted applications in adjoining areas of chemical and biological sciences, including liquid extraction,[1] sensing[2] and drug delivery.[3] The ITIES is by nature an electrified interface, hence the study of the various charge transfer processes across the interface can be achieved using electrochemical methods (e.g. cyclic voltammetry, amperometry, etc).[4] Consequently, it has been widely used as an analytical tool for different organic,[5] inorganic,[6] as well as biochemical[7] species. Many of these species are difficult to detect, with preferential selectivity, in a conventional metal/electrolyte electrochemical experiment.

A well-established approach to improve voltammetric measurements, and hence enhance the sensitivity of the detection tool, is through miniaturization of the interface, as suggested by Girault and co-workers.[8] In their work, they reduced the interface from a conventional macro-size (mm to cm diameter) into a micro-size interface (μm in diameter) by supporting the interface at the orifice of a pulled glass micropipette. Subsequent studies have explored miniaturization by supporting the ITIES on solid-state micro/nanoporous membranes, including track-etched polyester,[9] silicalite[10,11] and silicon nitride[12] membranes. The improvement which miniaturization can bring about derives from its elimination of the inherited drawbacks of macro-size ITIES, namely high impedance and charging current in the voltammetric measurements due to the resistance of the less polar organic phase. Moreover, it, more importantly, enhances the mass transfer due to the radial flux to the inlaid pore, leading to improvement in detection sensitivity.[13,14] In addition, if the modification of the ITIES is taken to its limit, through use of a nanoporous membrane, then the modified structure can impart both size and ion-selectivity via properly structured membranes.[10,14,15]

The modification of the ITIES can also be carried out with molecules or nanoparticles in either phase. Adsorption of nanoparticles at the ITIES can lead them to self-assemble into a uniform nanofilm.[16] Such a system has been found to have applications in reactions of relevance for energy conversion, namely oxygen reduction[17,18] and hydrogen evolution.[19,20] A similar model platform was also employed for ion transfer with Au,[21,22] silica[23,24] nanoparticles and carbon nanotubes[25] assembled at the interface. Nanoparticles were also employed to stabilise liquid | liquid microinterfaces. Opallo and Marken[26,27] used carbon nanoparticles to stabilise emulsions of micro-droplets of organic liquid at solid electrode surfaces, which

[a] H. A. Al Nasser, Prof. R. A. W. Dryfe
Department of Chemistry
The University of Manchester
Oxford Road, Manchester, U.K., M13 9PL
E-mail: robert.dryfe@manchester.ac.uk
[b] Dr. M. A. Bissett
Department of Materials
The University of Manchester
Oxford Road, Manchester, U.K., M13 9PL
[c] Dr. M. A. Bissett, Prof. R. A. W. Dryfe
Henry Royce Institute
The University of Manchester
Oxford Road, Manchester, U.K., M13 9PL

Special Collection An invited contribution to the Marcin Opałło Festschrift

were found to drive ion transfer processes between the organic and the aqueous phase at triple phase boundary junctions.

The nano-structure of the film formed at the ITIES is made up of a network of nanoparticles structures with voids, where their sizes depend on the size, shape and packing of the individual nanoparticles.[22,28,29] Therefore, adsorbed nanoparticles at the ITIES have been found to influence the ion transfer processes. In one way, they may act as a barrier with a blocking effect, nonetheless they could also enhance the selectivity of the target ion species and hence its transfer, depending on their interaction.

2D molybdenum disulphide (MoS_2) is one of the nanomaterials which has attracted considerable attention owing to its remarkable properties for different applications including water desalination,[30,31] power generation,[32] hydrogen evolution[20,33,34] and DNA translocation.[35,36] The last two applications were also studied with 2D films of MoS_2 adsorbed at the ITIES. Hirunpinyopas *et al.*[20] examined the hydrogen evolution at water|1,2-dichlorobenzene (DCB) interfaces catalysed by three 2D materials, namely graphene, WS_2 and MoS_2, and noticed the superiority of MoS_2 with the highest performance amongst them. For DNA sequencing, Feng *et al.*[37] showed that a system of viscosity gradient across MoS_2 nanopores can regulate the DNA translocation speed with highly specific ionic current signal-to-noise ratio. Using all-atom molecular dynamics, Shankla and Aksimentiev[38] demonstrated that the MoS_2 membrane can also shift the location of the liquid| liquid interface which in turns alters the physics of the nanopore translocation process.

In this paper, we explore the self-assembly of MoS_2 at the ITIES and investigate its electrochemical behaviour. We report on the formation of a MoS_2 film at the interface without the need for agitation or addition of co-solvents such as methanol or ethanol. Subsequently, we show how the film affects ion transfer across the water|DCB interface with a range of cations and anions of different sizes.

2. Results and Discussion

2.1. Synthesis of MoS_2 Nanosheets

Two exfoliation top-down methods were followed to prepare MoS_2 nanosheets, ultrasonic[20,39] and electrochemical[40] Li intercalation. The latter method provides MoS_2 nanosheets suspended in water, however, they were re-dispersed in DCB prior making the interfacial films for the electrochemical experiments. Although this exfoliation method is reported to provide an initial 1T-MoS_2 phase product, the nanosheets used in the electrochemical measurements are believed to be 2H-MoS_2 phase as revealed by UV-Vis and Raman spectra (Figure 1). The UV-Vis absorption spectrum shows B_1 (605 nm) and A_1 (665 nm) peaks which are a signature of 2H-MoS_2 phase.[41] On the other hand, the Raman spectrum provides two active modes A_{1g} (408 cm^{-1}) and $E_{2g}{}^1$ (383 cm^{-1}) but exhibits no additional shifts at around 150 (J_1), 226 (J_2) and 330 (J_3) cm^{-1} which are attributed to the longitudinal acoustic phonon modes of the 1T phase.[42] Since the 1T phase is not a stable form of MoS_2, it is therefore deduced that it has undergone a transformation into the 2H phase, given the time required to prepare the final nanosheets (~6 days) and the re-dispersion in an organic solvent (DCB). Extensive characterisation of the dispersions formed by these complementary approaches, ultrasonic[39] and electrochemical,[40] have been provided in earlier literature from our group:[20,40] as previously reported, the flakes generally have lateral dimensions in the sub-micron range for both routes, but the sonicated product is typically somewhat thicker than the few-layer product formed from the electrochemical approach.

2.2. Self-assembly of MoS_2 Nanosheets at ITIES

Two methods were pursued to prepare MoS_2 films at the ITIES for the ion transfer experiments. In the first method, which followed our previously reported procedure for interfacial assembly,[20] MoS_2 nanosheets were suspended in the organic phase, and the aqueous phase was poured on top of it. After that, the vial was sonicated for $\leq$60 seconds and left overnight to allow the nanosheets to self-assemble at the interface. In the second method, after adding the aqueous phase on top of the

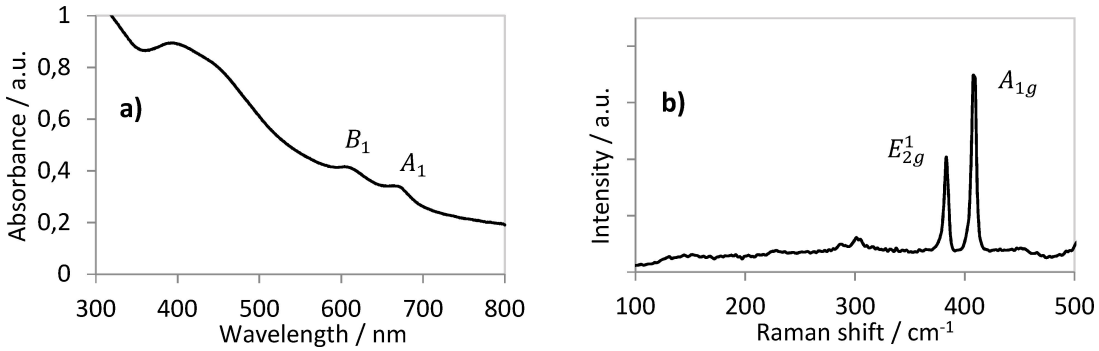

Figure 1. a) UV-Visible and **b)** Raman spectra of the electrochemically-exfoliated MoS_2 nanosheets after re-dispersion in DCB. The product from ultrasonic exfoliation method provided similar spectra.

organic phase, a certain amount of MoS_2 dispersion in DCB (solvent for the organic phase) was injected at the interface using a micropipette, and left overnight. Both methods were found to provide stable films at the water | DCB interface, which show a reasonable degree of spatial uniformity, as judged by optical microscopy (*vide infra*). However, the latter method has the advantage of eliminating the requirement of sonication/ mixing or addition of methanol/ethanol solvents which were usually used for the film formation.[22,29,43–45] In addition, it also provides a control over the amount/ number of nanoparticles which make up the film. It should be mentioned that relevant electrolytes (see below) were present in both phases whenever the nanofilms were prepared for the electrochemical measurements.

As a further investigation of the film formation, the adsorption of MoS_2 at the interface was attempted in the absence of both electrolytes. This resulted in agglomeration of the nanosheets at the centre of the interface instead of forming a uniform film covering the whole interface (Figure 2). In a previous study, Dryfe and co-workers[44] studied the effect of the electrolytes on the self-assembly of graphene at the interface, with a sonication step. They observed that graphene, besides adsorption at the interface, tends to attach at the walls of the glass cell. However, in the presence of the electrolytes (specifically the organic electrolyte) the wall attachment was not observed. These observations imply that the electrolyte can impact the energetics at ITIES and the surface tension of the whole system. Herein, the effect of the electrolytes was seen to be substantial, driving the self-assembly process of the MoS_2 nanosheets at the interface, in the absence of agitation or additional solution.

In order to specifically determine which electrolyte affects the self-assembly process, four separate vials containing different electrolyte combinations were prepared. Sodium chloride (NaCl) was used as the aqueous phase electrolyte, and bis (triphenylphosphoranylidene)ammonium tetrakis[3,5-bis (trifluoromethyl)phenyl] borate (BTPPATFPB) as the organic electrolyte. The electrolyte combinations were **a**) water | DCB, **b**) 10 mM $NaCl_{(aq)}$ | DCB, **c**) water | 10 mM $BTPPATFPB_{(DCB)}$ and **d**) 10 mM $NaCl_{(aq)}$ | 10 mM $BTPPATFPB_{(DCB)}$ (Figure 2i). In the presence of the aqueous electrolyte (vial **b**), no difference from vial **a** (absence of both electrolytes) was observed. In these vials, some of the nanosheets agglomerated at the interface while the rest remained suspended in the organic solvent with no wall attachments (Figure 2ii). However, in the presence of the organic electrolyte, MoS_2 nanosheets were seen to adsorb and self-assemble at the water | DCB interface forming a uniform film covering the whole interface. Thus, it is deduced that the organic electrolyte is the element which drives the attachment and self-assembly of the MoS_2 nanosheets at the interface, by changing the energetics and the surface tension of the whole system. The influence of the electrolytes highlights the change in interfacial structure when the particles form the film at the ITIES. Partial re-stacking occurs which forms a macroscopic film, with reasonably well-defined capillaries forming between the individual flakes, as judged from the size cut-off in ion sieving experiments.[20,31] The structure of the adsorbed film formed at the liquid-liquid interface is difficult to infer *in situ*, however the voltammetric data presented subsequently is used to shed some light on this point.

2.3. Transfer of Na^+

The general composition of the 4-electrode cell employed for investigating Na^+ transfer is shown in scheme 1. Figure 3a shows cyclic voltammograms (CVs) of Na^+ transfer across the water | DCB interface. In the absence of the ionophore dibenzo-18-crown-6 (DB18C6), the voltammogram consists of a "blank" potential window with limiting current from Na^+ and Cl^- transfer processes at the positive and negative Galvani potential differences, respectively, due to BTPPATFPB being more lipophilic than NaCl is hydrophilic.[46] Upon introducing the crown ether DB18C6 into the organic phase, it complexes with Na^+ at

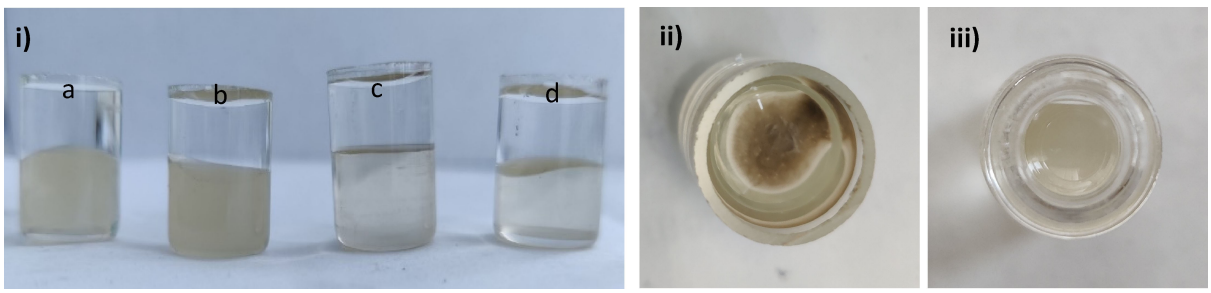

Figure 2. i) Attachment of MoS_2 nanosheets dispersed in DCB at the water | DCB interface after 24 hours. Different electrolyte combinations were present in each cell. **a)** water | DCB **b)** 10 mM $NaCl_{(aq)}$ | DCB, **c)** water | 10 mM $BTPPATFPB_{(DCB)}$ and **d)** 10 mM $NaCl_{(aq)}$ | 10 mM $BTPPATFPB_{(DCB)}$. **ii)** Top view of Cell (**a**). **iii)** Top view of Cell (**d**). Vial diameter = 1.5 cm.

Ag	AgCl	1 mM BTPPACl **Ref. water**	10 mM BTPPATFPB 1 mM dibenzo-18-crown-6 **DCB**	20 mM NaCl **water**	AgCl	Ag

Scheme 1. The composition of the ITIES cell used in the facilitated ion transfer studies.

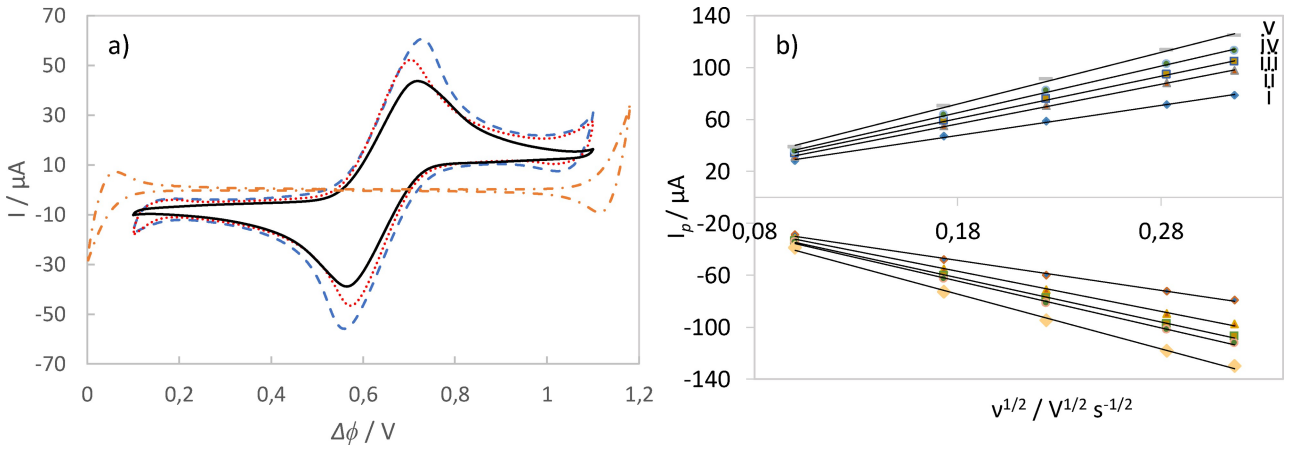

Figure 3. a) CVs for (—·) the supporting electrolytes; facilitated Na^+ ion transfer across (—) the plain and MoS_2-modified ITIES with initial concentrations of MoS_2 dispersion in DCB (…) 15 and (–) 35 mg/L, prepared by sonication method. Scan rate = 30 mV/s. **b)** Randles-Sevčik plot showing the linear relationship between the peak current (I_p) and the square root of the scan rate ($v^{1/2}$) for the facilitated Na^+ ion transfer across the plain and modified ITIES. The concentrations (mg/L) of MoS_2 dispersion in DCB are **i)** 0, **ii)** 15, **iii)** 23, **iv)** 35 and **v)** 50.

the interface leading to its facilitated transfer by lowering its Gibbs energy of transfer to a value corresponding to a potential within the potential window.[47] Since Na^+ is in excess compared to the organic phase ligand, the current is limited by the diffusion of DB18C6 from the bulk of the organic phase to the interface and the diffusion coefficient measured is in approximate agreement with that reported previously for this species.[48] Despite this, it can be seen that the peak-to-peak separation is large (> 59 mV), and was found to increase with increasing scan rate. This large separation is due to the residual uncompensated resistance arising from the low permittivity DCB phase, which is usually evident when working at centimetre-scale interfaces,[8] as in this experimental case (interfacial area = 0.64 cm^2).

Noticeably, Na^+ still transfers across the ITIES modified with MoS_2 nanosheets, which indicates that MoS_2 assemblies are permeable despite forming an apparently uniform film. Moreover, the peak current magnitude was found to increase slightly on increasing the concentration of the interfacial MoS_2; increasing the film's density and thickness. A Randles-Sevčik analysis of the data also showed an increase in the gradient of the linear fit with increasing concentration of interfacial MoS_2 (Figure 3b). Following the theory of voltammetry on partially blocked electrodes introduced by Amatore and co-workers,[49] partial coverage of the interface can provide either a similar or lower voltammetric response to that of a bare interface. The increase in the peak current with film thickness indicates that the transfer process across the interface is enhanced in the presence of interfacial MoS_2. Such an enhancement to the ion transfer might not be expected when considering the blockage of the interface by the sheets of MoS_2, thus leaving fewer pathways (uncovered areas) for ion passage, i.e. an attenuating effect on the ion transfer may be anticipated.

Set against the blocking effect of the film, the modest current enhancement indicates that the presence of MoS_2 nanosheets at the interface could lead to a net increase in its roughness, which leads to an increase in interfacial area. However, other studies on nanomaterials reported either unaltered or lower peak current responses upon introducing nanomaterials at the interface, e.g. carbon nanotubes[25] and gold nanoparticles.[22] Thus, even though the presence of nanomaterials at the interface increases the total interfacial area, its effect is not necessarily enough to induce a significant increase in the peak current.

In some earlier studies, it was found that the ion transfer enhancement was due to accumulation of the target ions near the interface. Mirčeski and co-workers[50,51] reported an increase in the peak current response for hydrophilic ion transfers across a cholesterol (amphiphilic molecule) modified water|nitrobenzene interface, due to the adsorption of the transferring ions onto cholesterol at the interface. In addition, using numerical simulations of mass transport across a solid-supported liquid|liquid micro-interface, Arrigan and co-workers[52,53] found that accumulation of transferring ions within the pores close to the interface led to an increase in the peak current in stripping voltammetry. Herein, it was speculated that sonication may lead to entrapping of the transferring ions within the nanosheets at the interface, hence making them readily available for transfer. As a way to eliminate this possibility, the second film formation method, which involves no sonication, was proposed. Yet again, the peak current was found to increase with increasing the film thickness (Figure 4a), which indicates that the ion transfer enhancement is not derived from the sonication itself.

The effect of MoS_2 nanosheets on the interfacial structure was further probed by optical microscopy (Figure 5). In a water|DCB system, small emulsified droplets/bubbles were found at the interface after 24 h. Upon introducing both electrolytes into this system, fewer droplets were seen at the interface, even when left overnight. However, when MoS_2 nanosheets were adsorbed at the interface, in the presence of both electrolytes, the emulsion droplets were retained at the interface. Furthermore, it was found that the number and size of the emulsion droplets were dependent on the concentration of MoS_2. The

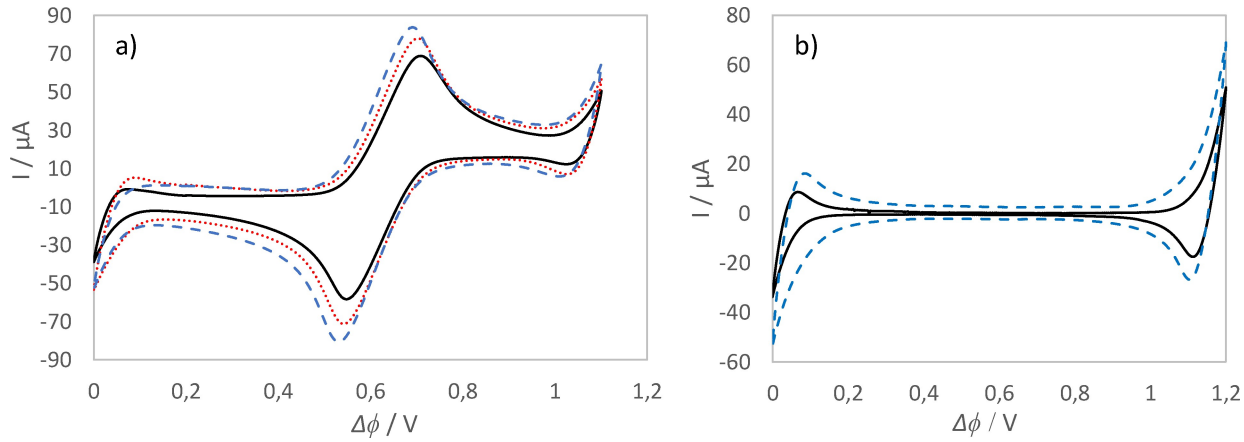

Figure 4. CVs obtained at the (—) plain and (… and –) MoS_2-modified ITIES by injection method **a)** with and **b)** without DB18C6 in the organic phase. Concentration of MoS_2 stock solution was 50 mg/L and the injected volumes were (…) 100 and (–) 300 µL. Scan rate = 50 mV/s.

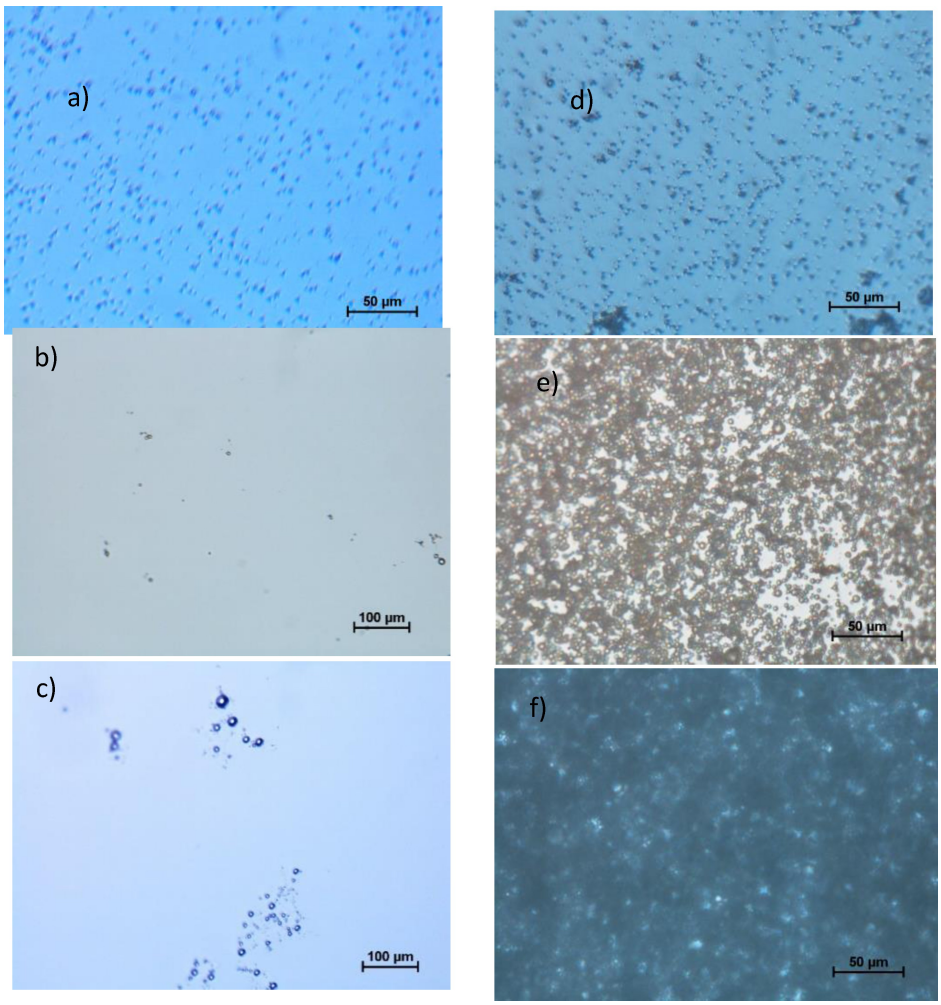

Figure 5. Optical micrographs of plain and modified ITIES of different compositions; **a)** water | DCB with no electrolytes. The remaining cells contained 20 mM $NaCl_{(aq)}$ | 10 mM $BTPPATFPB_{(DCB)}$ **b)** freshly made and **c)** after 24 h; and in the presence of MoS_2 film from different injections **d)** 50 uL, **e)** 100 uL and **f)** 300 uL. Concentration of MoS_2 stock solution = 50 mg/L.

influence of the electrolytes on bubble coalescence is well-established, where they can inhibit it or otherwise. Such inhibition is understood to depend on ion separation within the interfacial region and hence different electrolyte combinations would have different effects on bubble coalescence.[54,55] On the other hand, nanoparticles are known to play a key role in

stabilising emulsions at the interface. Stability of these emulsions depend on several factors, most of which are the wettability and surface properties of the nanoparticles and their interaction with the image charges in the water | oil system.[56,57] Thus, the interfacial film composed of multiple emulsion droplets is stabilised against coalescence by MoS_2 nanosheets. These emulsions increase the interfacial roughness, and given that 2H-MoS_2 is a semiconductor, it may be argued that the peak current enhancement may be reflected in the double layer capacitance contributed by the interfacial film. In regards to this argument, cyclic voltammetry was run in the absence of the ionophore to probe the effect of interfacial MoS_2 on the capacitive current (Figure 4b). While the capacitive current was found to increase in the presence of the interfacial film, its magnitude was not significant, insufficient to explain the enhanced Faradaic currents seen in the presence of the ionophore.

The new interfacial structure, which mediates the transfer route, potentially affects the voltammetric measurements. That is, the spherical micro-droplets at the interface influence the mass transport to the ITIES. As stated above, the modified ITIES with MoS_2 nanosheets contain more emulsion droplets than the bare ITIES, and hence alter the geometry of the interface. A different interfacial geometry would affect the mass transport and diffusion of ions from one phase to another. A macro-interface is reflected as a plane, in which the pathway of diffusion of the ions is linear. On the other hand, a micro-interface maintains a spherical or hemi-spherical interface, in which the transfer of the ions occurs by a radial diffusion process.[47] In this regard, a plain interface in a 4-electrode cell (area 0.64 cm^2) is a macro-interface while a modified interface can be thought of as a mix of macro- and micro-interface arrays, since it is covered by MoS_2-stabilised micro-droplets. Therefore, in the presence of MoS_2 at the interface, the peak current observed could consist of both linear (at planar parts) and radial (at spherical parts) diffusion processes towards and away from the interface. However, overlapping of diffusion layers is expected due to the random position and size of the spherical parts over the interface, leading to a peak-shaped voltammetric response. It is worth noting that, involvement of radial diffusion might be the cause of the increase in gradient of the linear fit of the Randles-Sevčik equation with increasing the concentration of MoS_2 at the interface because the whole surface (even though partially "blocked") can become active with respect to charge transfer.[49]

While this structure, which involves radial diffusion together with a larger interfacial area, is thought to enhance the ion transfer processes across the interface, it may not exclusively generate an enhancement to the peak current. Interfacial emulsions were also reported for adsorbed carbon nanotubes at the interface, yet the ion transfer across the interface was not enhanced.[25] Thus, the significant enhancement to the mass transport may also involve an interaction between the transferring ions with the adsorbed material. As discussed earlier, accumulation of transferring ions at the interface enhances their transfer. Several studies showed that MoS_2 nanosheets retain a net negative surface charge upon exfoliation.[58–61] The existence of such a negative charge was established as a result of several examples of cationic species being encapsulated in MoS_2 structure.[58,62–64] Studies related to the surface charge of MoS_2 nanosheets have also shown that their dispersion maintains a negative zeta potential.[65–68] In addition, exfoliation of MoS_2 results in numerous defects such as sulphur vacancies in its surface.[69,70] Remarkably, these vacancies were found to introduce gap states that allow favourable hydrogen adsorption, which in turns increases HER activity.[71,72] Recently, Pal and Barik[73] performed density functional theory simulations to study the impact of defects on mono- and layered-MoS_2. Interestingly, their calculations revealed high negative value of adsorption energies for Li^+ and Na^+ species at sulphur vacancies, which indicates that the presence of vacancies in MoS_2 surface promotes an energetically favourable interaction between the cations and layered-MoS_2. It is likely that the preferential cation transfer observed in this work is related to the surface charge of the exfoliated MoS_2 and associated favourable cation adsorption. In other words, the residual negative charge and the intrinsic defect structure of exfoliated MoS_2 cause accumulation of Na^+ ions at the modified ITIES, and hence enhancing the current due to their transfer.

XPS analysis was employed to investigate the presence of any ion species in the interfacial MoS_2 film after performing the electrochemical measurements (Figure 6). The XPS survey spectrum exhibits no peaks in the Na 1s region (1071-1071.5 eV), however, in the Cl 2p region, the peaks of Cl^- $2p_{3/2}$ and Cl^- $2p_{1/2}$ are present around 200.4 and 202.5 eV, respectively (Figure 6). The absence of Na^+ ions from the MoS_2 surface is more likely due to the washing procedure before the XPS measurements, and any intra-layer inclusions of Na would be difficult to detect in the surface-sensitive XPS technique. The chlorine species are believed to come from a strong organic solvent (DCB) adsorption and not the aqueous electrolyte (NaCl). This is because the $2p_{3/2}$ due to Cl^- is associated with a lower binding energy, around 198.4 eV, while the covalently bound chlorine is usually shifted to a higher binding energy above 200 eV.[74] In addition, adsorption of aromatic molecules on the flat basal plane of MoS_2 is favourable, with van der Waals interactions dominating the bonds between the π-conjugated ring and *p* orbitals of the surface sulphur atoms.[75,76] The negatively charged electron cloud of π systems interacts with positively charged ions in a favourable cation-π interactions.[77] Thus, the strongly physisorbed solvent molecules on the MoS_2 surface would reduce its blocking effect, and rather attract Na^+ ions into the interfacial film through π-cation interactions.

2.4. Transfer of TMA^+ and PF_6^- Ions

The permeability of the interfacial film was further investigated with larger ionic probes, namely Tetramethylammonium ion (TMA^+) and hexafluorophosphate ion (PF_6^-), which have reported ionic radii of 0.283 nm and 0.254 nm, respectively.[78] The opposing charges, but similar sizes, of these ions should allow the study of the charge and size selectivity of the interfacial film.

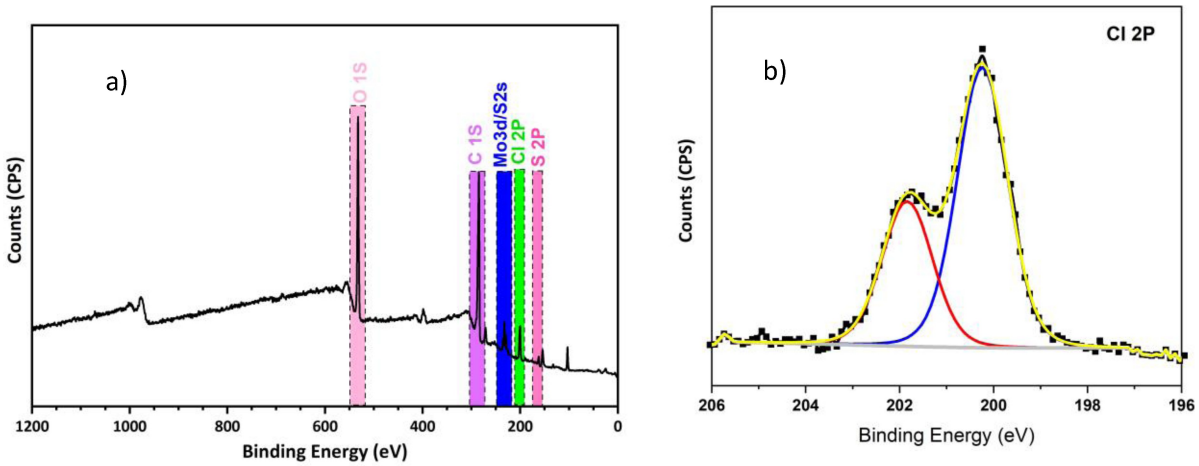

Figure 6. a) XPS survey spectrum of the MoS_2 nanosheets obtained from the water | DCB interface after the facilitated transfer of Na^+ ions across the interface. b) High-resolution XP spectrum of the Cl 2p region.

Ag	AgCl	1 mM BTPPACl **Ref. water**	10 mM BTPPATFPB **DCB**	10 mM LiCl 0.2 mM TMACl **water**	AgCl	Ag

Scheme 2. The composition of the ITIES cell used to study the transfer of TMA^+ ion. 0.2 mM $NaPF_6$ in aqueous phase was used to study the transfer of PF_6^- ion.

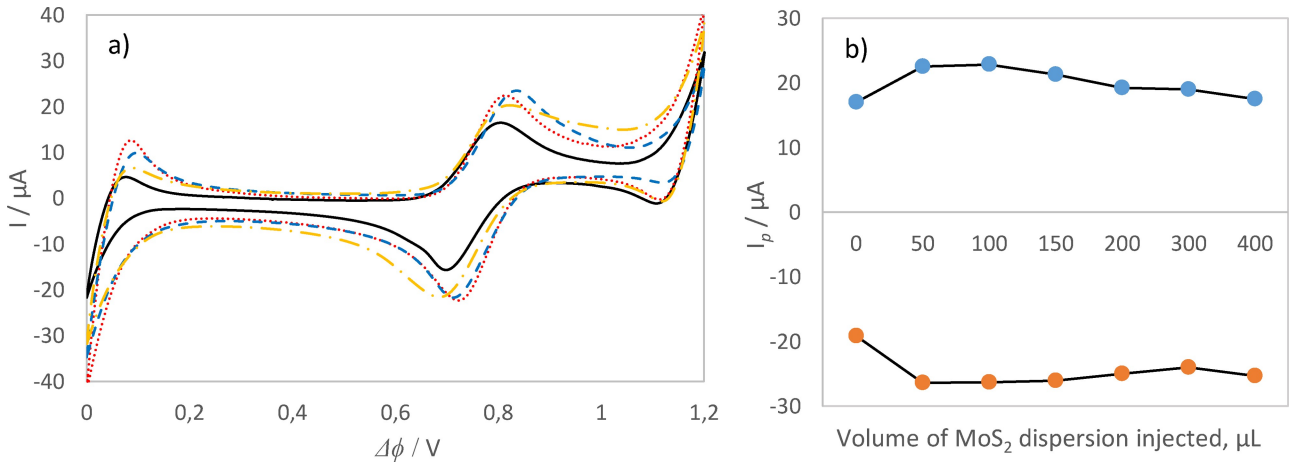

Figure 7. a) CVs of the plain and MoS_2-modified ITIES prepared by the injection method for the transfer of the TMA^+ ion. Volumes of MoS_2 dispersion injected were (—) 0, (…) 50, (–) 100 and (—·) 150 µL. **b)** Plot of the peak currents (forward and reverse) for the transfer of TMA^+ ion in relation to the amount of MoS_2 dispersion injected at the interface. Concentration of MoS_2 stock solution = 50 mg/L. Scan rate = 50 mV/s.

The composition of the electrochemical cell is shown in Scheme 2. Figure 7a shows CVs for the voltammetric transfer of TMA^+ across the plain interface, and in the presence of the interfacial MoS_2 film of differing thickness. The forward peak current was found to increase in the presence of a thin film at ITIES (up to 100 µL injection), however, the trend was seen to reverse with thicker interfacial films (Figure 7b). Thus, in the presence of few MoS_2 nanosheets at the interface, the transfer of TMA^+ across the interface is enhanced in a similar manner to that found with facilitated Na^+ transfer. As the interface becomes saturated with nanosheets, however, the film becomes thicker and denser, reducing the size of the ion pathways across the interface and hence retarding the passage of larger ions. On the other hand, the peak current of PF_6^- transfer was found to decrease in the presence of MoS_2 at the interface (Figure 8). Since the probe ions are of comparable size, this finding supports the above conclusion that the MoS_2 interfacial film exhibits some charge selectivity towards cationic species. This observation is consistent with the proposed mechanism for mass transport enhancement due to adsorption of MoS_2 at the interface, where the negative surface of MoS_2

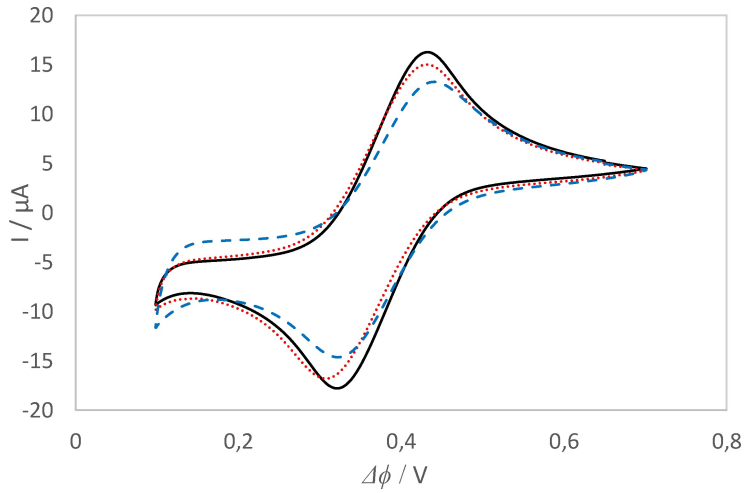

Figure 8. CVs of the plain and MoS_2-modified ITIES prepared by injection method for the transfer of PF_6^- ion. Volume of MoS_2 dispersion injected were (—) 0, (…) 50 and (–) 100 μL. Concentration of MoS_2 stock solution = 50 mg/L. Scan rate = 50 mV/s.

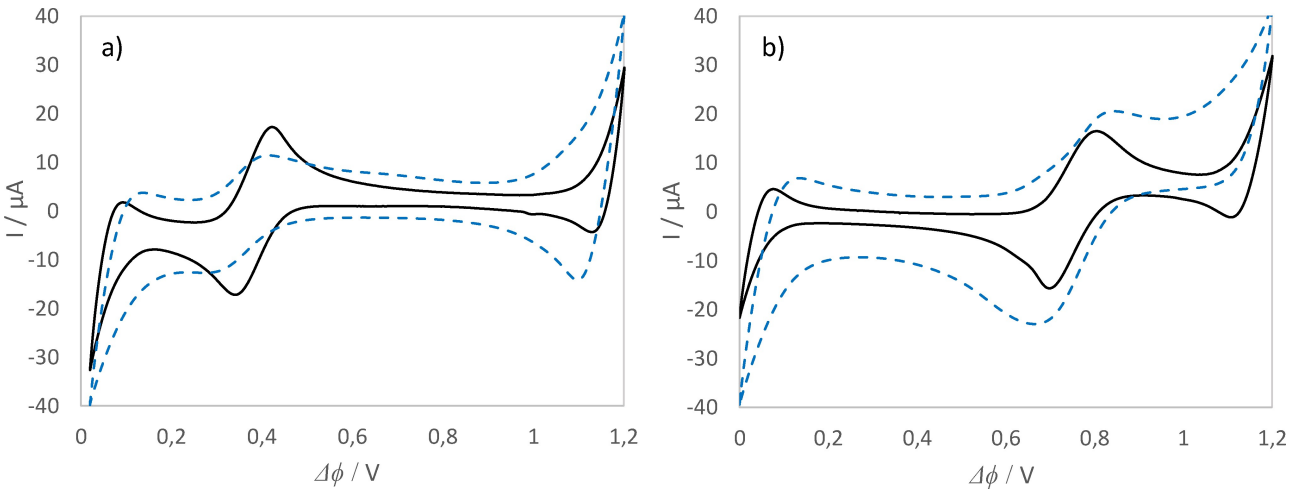

Figure 9. CVs of the plain and MoS_2-saturated interfaces prepared by injection method for the transfer of **a)** PF_6^- and **b)** TMA^+ ions. Volume of MoS_2 dispersion injected were (–) 300 and (–) 400 μL for the transfer of PF_6^- and TMA^+ ions, respectively. Concentration of MoS_2 stock solution = 50 mg/L. Scan rate = 50 mV/s.

nanosheets leads to accumulation of the cationic species at the interface.

Remarkably, as the film becomes more saturated, the micro-interface features become more pronounced. Recalling the theory of partially blocked electrodes, excessive fractional film coverage, close to unity, of the electrode surface leads to non-linear diffusion effects.[49] Similarly, micro-ITIES maintain a semi-spherical interface which results in steady-state conditions of mass transport.[8,9] It was noticed that with excessive amounts of MoS_2 nanosheets at the interface, the voltammetric response of the peak current for PF_6^- transfer changes from a peak-shaped into a sigmoidal response (Figure 9a). This observation is again consistent with the involvement of radial diffusion of the ions to the interface in the presence of interfacial MoS_2. On the other hand, while the forward (positive) current for TMA^+ transfer was found to plateau and its magnitude decreased with subsequent saturation, the reverse peak seemed unaffected, retaining its peak shape (Figure 9b). Numerical modelling of ion transfers across micro-ITIES by Molina *et al.*[79] showed that the asymmetry of the forward and reverse peaks implies the existence of capillary-like interfacial structures. This characteristic shape of the CV was also established experimentally in solid-supported micro-ITIES.[9,15,80] In a microporous membrane, one phase usually fills the pores preferentially, leading to diffusion zones of different dimensions within and outside the pores. Therefore, diffusion zones of the TMA^+ species from water to the organic phase and vice versa are different. That is, while the radial diffusion outside the capillary structure (formed between the restacked MoS_2 flakes) governs the forward transfer of the cationic species, linear diffusion inside the capillary controls the return of the species to the original phase. Consequently, it can be deduced that the organic phase primarily fills the capillaries, and the location of the interface is either at the capillary mouth and on the aqueous side of the

film or slightly recessed within the channel. The overall picture we have established of the structure of the MoS_2 film formed at the ITIES is incomplete and will require further structural and dynamic (e.g. via ac impedance measurements) but the voltammetric and optical data obtained so far suggest that a charged film is formed, exhibiting a preference for cation transfer, and the formation of persistent emulsions increases the net interfacial area. A schematic diagram is provided in Figure 10.

3. Conclusion

MoS_2 films were prepared at the water|DCB interface using an injection method of the exfoliated nanosheets at the interface, and without the involvement of sonication or an additional solvent. The organic electrolyte BTPPATFPB was found to drive the self-assembly process, possibly by changing the energetics at the ITIES and the surface tension of the system. Optical microscopy revealed that the film is composed of multiple emulsified droplets stabilised by MoS_2, where their number and size increase with increasing amount of MoS_2 dispersion injected at the interface. The voltammetric measurements showed that the MoS_2 film is permeable, and significantly enhances the transfer of Na^+ ions across ITIES. The film also exhibited a charge selectivity for the TMA^+ ion over the PF_6^- ion, which are of comparable size. This selectivity is believed to stem, primarily, from accumulation of the aqueous cationic species at the interface as a result of the structural defects and the residual negative charge of the MoS_2 nanosheets. In addition, the micro-structure of the film is anticipated to increase the interfacial area and influence the diffusion regimes across the interface leading to radial diffusion conditions of mass transport. Involvement of such radial diffusion process was evident when transferring PF_6^- and TMA^+ ions across saturated interfacial films, where the peak-shaped response changed into a sigmoidal response in a similar manner to that found in solid-state micro-ITIES.

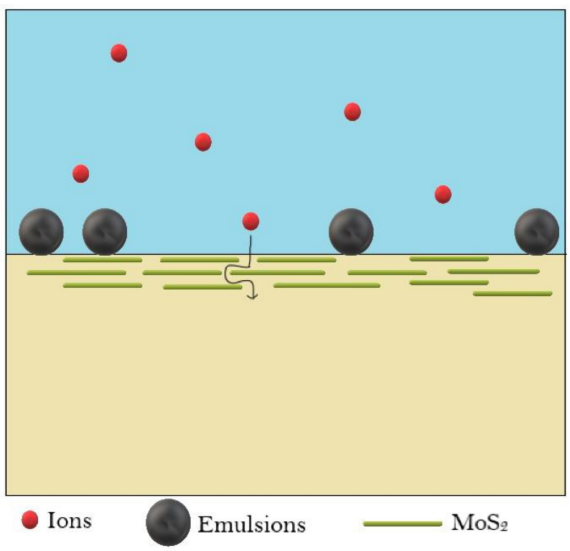

Figure 10. Schematic diagram for ion transfer across a modified ITIES with an interfacial layer of MoS_2 nanosheets. The sizes of the individual components are not drawn to scale.

The MoS_2 films also exhibit size-selectivity depending on the size of the transferring ion and the thickness of the film. Adsorbing MoS_2 at the interface resulted in enhancement of the transfer of TMA^+ ion across the interface, but as the interfacial MoS_2 coverage increased further, TMA^+ ion transfer from water to DCB was retarded.

The charge and size perm-selectivity of MoS_2 films at ITIES foster current knowledge about the nanomaterial and assist in elucidating the transport mechanism within such membranes. Future studies will focus on the application of complementary techniques, such as a.c. impedance, to understand the structure of the MoS_2-modified ITIES. Moreover, current results promote the use of MoS_2 in extraction, sensing and detection applications. The charge selectivity of MoS_2 films can be manipulated through, for example, functionalisation.[31] The size selectivity can be controlled through proper evaluation for the film thickness and density. Future work will approach manipulating the selectivity of these films through functionalisation. In addition, ion transfer across solid-state micro-ITIES modified with MoS_2 will be explored to produce robust, scalable membranes.

Experimental Section

Chemicals and Materials

Molybdenum (IV) sulphide (MoS_2, powder, ~6 μm) sodium chloride (NaCl, ≥99%), lithium chloride (LiCl, ≥99%), tetramethylammonium chloride (TMACl, 99%), sodium hexafluorophosphate ($NaPF_6$, 99.99%) and bis (triphenylphosphoranylidene)ammonium chloride (BTPPACl) were purchased from Sigma-Aldrich. 1,2-dichlorobenzene (DCB, 99%) and Sodium tetrakis[3,5-bis(triflormethyl) phenyl]borate (NaTFPB) were purchased from Alfa Aesar. Dibenzo-18-crown-6 (DB18C6, 98%) was aproduct of Lancaster Synthesis. All chemicals were used without further purification. NaTFPB and BTPPACl were reacted by metathesis to give the organic electrolyte, BTPPATFPB, as described previously.[81] Ultrapure water (18.2 MΩ cm resistivity, Milli-Q Direct 8, Merck Millipore, USA) was used for aqueous solutions preparation. Silver wire (1 mm diameter) and platinum mesh (plain weave wire diameter 0.1 mm, aperture size 0.39 mm, open area 62.7%, 420 cm^2) were purchased from Advent Research Materials Ltd.

Equipment

An Ultrasonic bath (Elmasonic P 70H, 230–240 V with max. power 820 W, Elma Hans Schmidbauer GmbH & Co., Germany) was used to exfoliate MoS_2 in DCB. The temperature during sonication was controlled by a Recirculating Cooler (F250, Julabo GmbH, Temperature Control Company, Germany). A potentiostat (Metrohm Autolab B.V., PGSTAT302N, Netherlands) was used to carry out the electrochemical exfoliation of MoS_2 and all electrochemical experiments at liquid|liquid interfaces. A Benchtop centrifuge (Sigma Laborzentrifugen GmbH, Germany) was used to centrifuge exfoliated materials. DH-2000-BAL UV-visible spectrometer using a deuterium-halogen light source (Ocean Optics, Germany) was used to collect the UV-visible absorption spectra. Raman spectroscopy at

an excitation wavelength of 532 nm was used to characterise the exfoliated nanosheets using a Renishaw inVia confocal Raman spectrometer. X-ray photoelectron spectroscopy (XPS) was carried out in a Specs UHV system. The photoejected electrons were excited using a monochromatic Al Kα (1486.6 eV) source operating at 120 W and analyzed using a Phiobos 150 electron energy analyzer operating at 30 eV pass energy. A Motic Stereo Digital Microscope (The Microscope Store, L.L.C., USA) was used to record micrographs after the assembly of 2D materials at the interfaces.

MoS_2 Dispersions in DCB and Their Concentrations

Synthesis of MoS_2 nanosheets via ultrasonic exfoliation was already performed in DCB, and hence they were only centrifuged for the supernatant solution as previously reported.[20] Exfoliation of the electrochemically Li-intercalated MoS_2 occurred in water. They were filtered and dried as previously reported.[40] Then, they were re-dispersed in 100 mL DCB, and sonicated in a water bath for 30 min to disaggregate the nanosheets. After that, they were centrifuged twice at 1500 rpm for 30 minutes to sediment the non-exfoliated material, and hence the supernatant solution containing the nanosheets was collected.

The concentration of the exfoliated MoS_2 was determined by filtering three samples of the dispersion onto PVDF membranes (hydrophilic, 0.1 μm pore) using a Swinnex Filter Holder connected to a Luer Lock Syringe. The membranes were then left to dry for 3 days at room temperature before weighing them, and the average concentration was calculated in mg/L.

Electrochemical Measurements

The cyclic voltammetric measurements were performed by using a four-electrode setup, with a Pt-mesh counter electrode (CE) and a Ag/AgCl reference electrode (RE) in each liquid phase. The potentiostat was used to control the Galvani potential and monitor the passage of current. The standard ITIES setup used a three-arm cell, with two capillary arms for the REs and a third arm allowing direct access to the DCB phase for a CE without disruption of the liquid | liquid interface. The aqueous RE was inserted through the open top of the cell. The data were analysed by using Nova 1.10 software.

Acknowledgements

H. A. N. wishes to acknowledge funding from the Ministry of Education, Saudi Arabia. R. A. W. D. thanks the EPSRC (UK, grant reference EP/R023034/1) for financial support.

Conflict of Interest

The authors declare no conflict of interest.

Keywords: liquid-liquid interfaces · MoS_2 · ion transfer · interfacial films · nanosheets

[1] A. Berduque, A. Sherburn, M. Ghita, R. A. W. Dryfe, D. W. M. Arrigan, *Anal. Chem.* **2005**, *77*, 7310–7318.
[2] E. D. Burgoyne, T. J. Stockmann, A. F. Molina-Osorio, R. Shanahan, G. P. McGlacken, M. D. Scanlon, *J. Phys. Chem. C* **2019**, *123*, 24643–24650.
[3] W. Wang, H. Qi, T. Zhou, S. Mei, L. Han, T. Higuchi, H. Jinnai, C. Y. Li, *Nat. Commun.* **2016**, *7*, 10599.
[4] R. A. W. Dryfe, *Advances in Chemical Physics, (Wiley), Vol. 141*, **2009**, pp 153–215.
[5] G. Herzog, V. Kam, A. Berduque, D. W. M. Arrigan, *J. Agric. Food Chem.* **2008**, *56*, 4304–4310.
[6] A. M. O'Mahony, M. D. Scanlon, A. Berduque, V. Beni, D. W. M. Arrigan, E. Faggi, A. Bencini, *Electrochem. Commun.* **2005**, *7*, 976–982.
[7] D. W. M. Arrigan, M. Ghita, V. Beni, *Chem. Commun.* **2004**, 732–733.
[8] G. Taylor, H. H. J. Girault, *J. Electroanal. Chem. Interfacial Electrochem.* **1986**, *208*, 179–183.
[9] R. A. W. Dryfe, B. Kralj, *Electrochem. Commun.* **1999**, *1*, 128–130.
[10] M. J. Stephenson, A. J. King, S. M. Holmes, R. A. W. Dryfe, *J. Phys. Chem. B* **2005**, *109*, 19377–19384.
[11] G. C. Lillie, R. A. W. Dryfe, S. M. Holmes, *Analyst* **2001**, *126*, 1857–1860.
[12] M. D. Scanlon, J. Strutwolf, A. Blake, D. Iacopino, A. J. Quinn, D. W. M. Arrigan, *Anal. Chem.* **2010**, *82*, 6115–6123.
[13] M. Rimboud, R. D. Hart, T. Becker, D. W. M. Arrigan, *Analyst* **2011**, *136*, 4674–4681.
[14] X. Huang, L. Xie, X. Lin, B. Su, *Anal. Chem.* **2016**, *88*, 6563–6569.
[15] R. Zazpe, C. Hibert, J. O'Brien, Y. H. Lanyon, D. W. M. Arrigan, *Lab Chip* **2007**, *7*, 1732–1737.
[16] S. Biswas, L. T. Drzal, *Nano Lett.* **2009** *9*, 167–172.
[17] A. N. J. Rodgers, R. A. W. Dryfe, *ChemElectroChem* **2016**, *3*, 472–479.
[18] Y. Gründer, M. D. Fabian, S. G. Booth, D. Plana, D. J. Fermín, P. I. Hill, R. A. W. Dryfe, *Electrochim. Acta* **2013**, *110*, 809–815.
[19] J. J. Nieminen, I. Hatay, P. Ge, M. A. Méndez, L. Murtomäki, H. H. Girault, *Chem. Commun.* **2011**, *47*, 5548–5550.
[20] W. Hirunpinyopas, A. N. J. Rodgers, S. D. Worrall, M. A. Bissett, R. A. W. Dryfe, *ChemNanoMat* **2017**, *3*, 428–435.
[21] N. Younan, M. Hojeij, L. Ribeaucourt, H. H. Girault, *Electrochem. Commun.* **2010**, *12*, 912–915.
[22] E. Smirnov, P. Peljo, M. D. Scanlon, H. H. Girault, *ACS Nano* **2015**, *9*, 6565–6575.
[23] L. Poltorak, G. Herzog, A. Walcarius, *Electrochem. Commun.* **2013**, *37*, 76–79.
[24] M. C. Collins, M. Hébrant, G. Herzog, *Electrochim. Acta* **2018** *282*, 155–162.
[25] A. K. Rabiu, P. S. Toth, A. N. J. Rodgers, R. A. W. Dryfe, *ChemistryOpen* **2017**, *6*, 57–63.
[26] S. M. MacDonald, P. D. I. Fletcher, Z.-G. Cui, M. Opallo, J. Chen, F. Marken, *Electrochim. Acta* **2007**, *53*, 1175–1181.
[27] K. Lawrence, C. L. Baker, T. D. James, S. D. Bull, R. Lawrence, J. M. Mitchels, M. Opallo, O. A. Arotiba, K. I. Ozoemena, F. Marken, *Chem. Asian J.* **2014**, *9*, 1226–1241.
[28] V. Divya, M. V. Sangaranarayanan, M. V. J. Nanosci, *Nanotechnology* **2015**, *15*, 6863–6882.
[29] J. Neilson, M. P. Avery, B. Derby, *ACS Appl. Mater. Interfaces* **2020**, *12*, 25125–25134.
[30] M. Heiranian, A. B. Farimani, N. R. Aluru, *Nat. Commun.* **2015**, *6*, 8616.
[31] W. Hirunpinyopas, E. Prestat, S. D. Worrall, S. J. Haigh, R. A. W. Dryfe, M. A. Bissett, *ACS Nano* **2017**, *11*, 11082–11090.
[32] J. Feng, M. Graf, K. Liu, D. Ovchinnikov, D. Dumcenco, M. Heiranian, V. Nandigana, N. R. Aluru, A. Kis, A. Radenovic, *Nature* **2016**, *536*, 197–200.
[33] M. A. Lukowski, A. S. Daniel, F. Meng, A. Forticaux, L. Li, S. Jin, *J. Am. Chem. Soc.* **2013**, *135*, 10274–10277.
[34] I. Hatay, P. Y. Ge, H. Vrubel, X. Hu, H. H. Girault, *Energy Environ. Sci.* **2011**, *4*, 4246–4251.
[35] K. Liu, J. Feng, A. Kis, A. Radenovic, *ACS Nano* **2014**, *8*, 2504–2511.
[36] A. B. Farimani, K. Min, N. R. Aluru, *ACS Nano* **2014**, *8*, 7914–7922.
[37] J. Feng, K. Liu, R. D. Bulushev, S. Khlybov, D. Dumcenco, A. Kis, A. Radenovic, *Nat. Nanotechnol.* **2015**, *10*, 1070–1076.
[38] M. Shankla, A. Aksimentiev, *ACS Appl. Mater. Interfaces* **2020**, *12*, 26624–26634.
[39] J. N. Coleman, M. Lotya, A. O'Neill, S. D. Bergin, P. J. King, U. Khan, K. Young, A. Gaucher, S. De, R. J. Smith, I. V. Shvets, S. K. Arora, G. Stantonl, H.-Y. Kim, K. Lee, G. T. Kim, G. S. Duesberg, T. Hallam, J. J. Boland, J. J. Wang, J. F. Donegan, J. C. Grunlan, G. Moriarty, A. Shmeliov, R. J. Nicholls, J. M. Perkins, E. M. Grieveson, K. Theuwissen, D. W. McComb, P. D. Nellist, V. Nicolosi, *Science.* **2011**, *331*, 568–571.
[40] A. Ejigu, I. A. Kinloch, E. Prestat, R. A. W. Dryfe, *J. Mater. Chem. A* **2017**, *5*, 11316–11330.
[41] J. A. Wilson, A. D. Yoffe, *Adv. Phys.* **1969**, *18*, 193–335.

[42] S. Jiménez Sandoval, D. Yang, R. F. Frindt, J. C. Irwin, *Phys. Rev. B* **1991**, *44*, 3955–3962.
[43] Y.-K. Park, S.-H. Yoo, S. Park, *Langmuir* **2007**, *23*, 10505–10510.
[44] A. N. J. Rodgers, A. K. Rabiu, P. S. Toth, R. W. Adams, R. A. W. Dryfe, *Electrochim. Acta* **2019**, *308*, 307–316.
[45] W. M. R. Divigalpitiya, R. F. Frindt, S. R. Morrision, *Science* **1989**, *246*, 369–371.
[46] N. E. A. Cousens, A. R. Kucernak, *Electrochem. Commun.* **2011**, *13*, 1539–1541.
[47] Y. Shao, M. D. Osborne, H. H. Girault, *J. Electroanal. Chem. Interfacial Electrochem.* **1991**, *318*, 101–109.
[48] X. Han, Z. Zhang, S. Dong, E. Wang, *Electroanalysis* **2004**, *16*, 1014–1018.
[49] C. Amatore, J.-M. Savéant, D. Tessier, *J. Electroanal. Chem. Interfacial Electrochem.* **1983**, *147*, 39–51.
[50] F. Quentel, V. Mirčeski, M. L'Her, F. Spasovski, M. Gaćina, *Electrochem. Commun.* **2007**, *9*, 2489–2495 .
[51] V. Mirceski, B. Mitrova, V. Ivanovski, N. Mitreska, A. Aleksovska, R. Gulaboski, *J. Solid State Electrochem.* **2015**, *19*, 2331–2342.
[52] J. Strutwolf, D. W. M. Arrigan, *Anal. Bioanal. Chem.* **2010**, *398*, 1625–1631.
[53] J. Strutwolf, M. D. Scanlon, D. W. M. Arrigan, *J. Electroanal. Chem.* **2010**, *641*, 7–13.
[54] S. Marčelja, *Curr. Opin. Colloid Interface Sci.* **2004**, *9*, 165–167.
[55] C. L. Henry, C. N. Dalton, L. Scruton, V. S. J. Craig, *J. Phys. Chem. C* **2007**, *111*, 1015–1023.
[56] M. E. Leunissen, A. van Blaaderen, A. D. Hollingsworth, M. T. Sullivan, P. M. Chaikin, *Proc. Nat. Acad. Sci.* **2007**, *104*, 2585–2590.
[57] J. Wu, G.-H. Ma, *Small* **2016**, *12*, 4633–4648.
[58] M. Danot, J. L. Mansot, A. S. Golub, G. A. Protzenko, P. B. Fabritchnyi, Y. N. Novikov, J. Rouxel, *Mater. Res. Bull.* **1994**, *29*, 833–841.
[59] A. S. Golub, I. B. Shumilova, Y. V. Zubavichus, M. Jahncke, G. Süss-Fink, M. Danot, Y. N. Novikov, *J. Mater. Chem.* **1997**, *7*, 163–167.
[60] T.-W. Lee, C.-C. Chen, C. Chen, *Environ. Sci. Technol.* **2019**, *53*, 6282–6291.
[61] J. Heising, M. G. Kanatzidis, *J. Am. Chem. Soc.* **1999**, *121*, 11720–11732.
[62] H. Tagaya, T. Hashimoto, M. Karasu, T. Izumi, K. Chiba, *Chem. Lett.* **1991**, *20*, 2113–2116.
[63] S. Nakagaki, A. S. Mangrich, F. A. Wypych, *Inorg. Chim. Acta* **1997**, *254*, 213–217.
[64] J. Brenner, C. L. Marshall, L. Ellis, N. Tomczyk, J. Heising, M. Kanatzidis, *Chem. Mater.* **1998**, *10*, 1244–1257.
[65] L. Sun, H. Huang, X. Peng, *Chem. Commun.* **2013**, *49*, 10718–10720.
[66] W. Hirunpinyopas, E. Prestat, P. Iamprasertkun, M. A. Bissett, R. A. W. Dryfe, *2D Mater.* **2019**, *7*, 15030.
[67] W.-M. Huang, W.-S. Liao, Y.-M. Lai, I.-W. P. Chen, *J. Mater. Chem. C* **2020**, *8*, 510–517.
[68] Z. Wang, Q. Tu, A. Sim, J. Yu, Y. Duan, S. Poon, B. Liu, Q. Han, J. J. Urban, D. Sedlak, B. Mi, *Environ. Sci. Technol.* **2020**, *54*, 12602–12611.
[69] P. Vancsó, G. Z. Magda, J. Pető, J.-Y. Noh, Y.-S. Kim, C. Hwang, L. P. Biró, L. Tapasztó, *Sci. Rep.* **2016**, *6*, 29726.
[70] M. J. ParK, S. Gravelsins, J. Son, A. M. van der Zande, A.-A. Dhirani, *ACS Nano* **2019**, *13*, 6469–6476.
[71] H. Li, C. Tsai, A. L. Koh, L. Cai, A. W. Contryman, A. H. Fragapane, J. Zhao, H. S. Han, H. C. Manoharan, F. Abild-Pedersen, J. K. Nørskov, X. Zheng, *Nat. Mater.* **2016**, *15*, 48–53.
[72] L. Wu, N. Y. Dzade, M. Yu, B. Mezari, A. J. F. van Hoof, H. Friedrich, N. H. de Leeuw, E. J. M. Hensen, J. P. Hofmann, *ACS Energy Lett.* **2019**, *4*, 1733–1740.
[73] G. Barik, S. Pal, *J. Phys. Chem. C* **2019**, *123*, 21852–21865.
[74] J. F. Moulder, W. F. Stickle, P. E. Sobol, K. D. Bomben, *Handbook of X-ray Photoelectron Spectroscopy*. (Perkin-Elmer Corporation, **1992**).
[75] P. G. Moses, J. J. Mortensen, B. I. Lundqvist, J. K. Nørskov, *J. Chem. Phys.* **2009**, *130*, 104709.
[76] J. Song, M. Li, H. Liang, H. Lou, *Comput. Theor. Chem.* **2017**, *1118*, 115–122.
[77] A. S. Mahadevi, G. N. Sastry, *Chem. Rev.* **2013**, *113*, 2100–2138.
[78] M. Ue, *J. Electrochem. Soc.* **1994**, *141*, 3336–3342.
[79] A. Molina, E. Laborda, R. G. Compton, *J. Phys. Chem. C* **2014**, *118*, 18249–18256.
[80] S. Peulon, V. Guillou, M. L'Her, *J. Electroanal. Chem.* **2001**, *514*, 94–102.
[81] F. Reymond, V. Chopineaux-Courtois, G. Steyaert, G. Bouchard, P.-A. Carrupt, B. Testa, H. H. Girault, *J. Electroanal. Chem.* **1999**, *462*, 235–250.

Manuscript received: June 15, 2021
Revised manuscript received: August 8, 2021

ARTICLES